J Physiol Sci (2012) 62:11–19
DOI 10.1007/s12576-011-0180-9

ORIGINAL PAPER

Comparison of the effects of continuous and pulsatile left ventricular-assist devices on ventricular unloading using a cardiac electromechanics model

Ki Moo Lim · Jason Constantino · Viatcheslav Gurev · Renjun Zhu · Eun Bo Shim · Natalia A. Trayanova

Received: 15 September 2011 / Accepted: 23 October 2011 / Published online: 11 November 2011

Abstract Left ventricular-assist devices (LVADs) are used to supply blood to the body of patients with heart failure. Pressure unloading is greater for counter-pulsating LVADs than for continuous LVADs. However, several clinical trials have demonstrated that myocardial recovery is similar for both types of LVAD. This study examined the contractile energy consumption of the myocardium with continuous and counter-pulsating LVAD support to ascertain the effect of the different LVADs on myocardial recovery. We used a three-dimensional electromechanical model of canine ventricles, with models of the circulatory system and an LVAD. We compared the left ventricular peak pressure (LVPP) and contractile ATP consumption between pulsatile and continuous LVADs. With the continuous and counter-pulsating LVAD, the LVPP decreased to 46 and 10%, respectively, and contractile ATP consumption decreased to 60 and 50%. The small difference between the contractile ATP consumption of these two types of LVAD may explain the comparable effects of the two types on myocardial recovery.

Keywords Circulatory system · Electromechanical model · Left ventricular-assist device · Counter pulsating · ATP consumption

K. M. Lim · E. B. Shim (✉)
Department of Mechanical and Biomedical Engineering, Kangwon National University, Chuncheon, Kangwon-do, Republic of Korea
e-mail: ebshim@kangwon.ac.kr

J. Constantino · V. Gurev · R. Zhu · N. A. Trayanova
Institute for Computational Medicine and the Department of Biomedical Engineering, Johns Hopkins University, Baltimore, MD 21218, USA

Introduction

For patients with end-stage heart failure (HF), left ventricular-assist devices (LVADs) are used as a bridge to transplantation [1, 2] or destination therapy [3], restoring normal cardiac output and blood pressure. An LVAD may also help myocardial function to recover, as myocardial recovery with LVAD support has been documented clinically on the basis of reduced left ventricular mass [4, 5] and heart chamber size [5, 6], improved mitral filling [7], and regression of cardiomyocyte hypertrophy [6, 7].

A variety of studies have compared the hemodynamic benefits of continuous versus pulsatile LVAD pumps [8–10]. A pulsatile LVAD provides greater ventricular unloading in the pressure and volume of the left ventricle (LV) than the continuous variety, because of counter-pulsation, i.e. the synchronization of the pumping phase with the LV contraction [11, 12]. Nevertheless, myocardial recovery is comparable for both types [13]. This indicates that pressure and volume unloading may not be the main factors underlying myocardial recovery, and other effects of LVADs should be considered to determine the best LVAD strategy to optimize recovery.

In addition to the pressure and volume unloading, reduction in myocardial energy consumption is an important aspect of myocardial recovery. Therefore, to compare the performance of pulsatile and continuous LVADs in respect of myocardial recovery, it is important to quantify the reduction in the contractile energy consumption of the myocardium during LVAD support. However, experimental methods [14] to document and evaluate myocardial energy consumption throughout the ventricular volume are hampered by low spatiotemporal resolution. Computational modeling is an alternative approach that overcomes this limitation.

We have previously developed a computational model of LVAD support, and showed that a pulsatile LVAD under counter-pulsation conditions provided more pressure unloading and coronary perfusion than did a continuous-type LVAD [11]. However, heart function in the model was represented by a time-varying capacitance, making it was impossible to quantify the changes in the local contractile energy consumption of the myocardium. We recently developed a three-dimensional (3D) electromechanical model of failing canine ventricles together with a lumped model of the circulatory system [15, 16]. In this study, we combine the electromechanical model with a lumped model of an LVAD to investigate changes in the contractile energy consumption of the myocardium with continuous and with counter-pulsating LVAD support to ascertain the effects of different LVADs on myocardial recovery.

Methods

To construct an integrated model of an LVAD implanted in the cardiovascular system, we combined the 3D image-based electromechanical model of failing canine ventricles [15] with a lumped model of the circulatory system and LVAD function [11]. A schematic diagram of the integrated model is shown in Fig. 1.

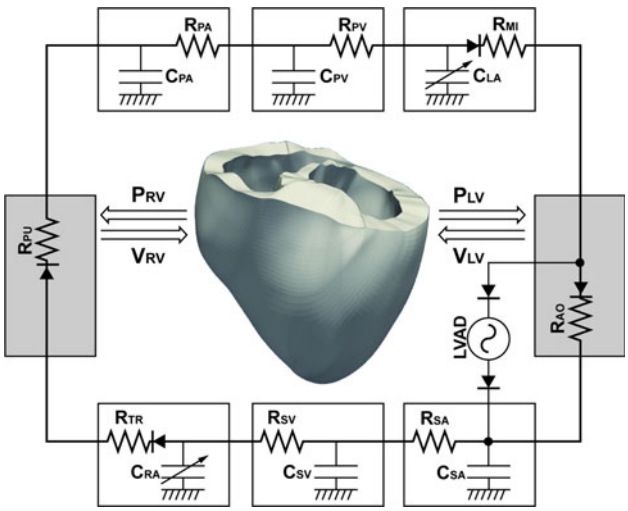

Fig. 1 Schematic diagram of the finite-element ventricular electromechanical model coupled with the circulatory and LVAD models. P_{RV} RV pressure, V_{RV} RV volume, P_{LV} LV pressure, V_{LV} LV volume, R_{PA} pulmonary artery resistance, C_{PA} pulmonary artery compliance, R_{PV} pulmonary vein resistance, C_{PV} pulmonary vein compliance, R_{MI} mitral valve resistance, C_{LA} left atrium compliance, R_{AO} aortic valve resistance, R_{SA} systemic artery resistance, C_{SA} systemic artery compliance, R_{SV} systemic vein resistance, C_{SV} systemic vein compliance, R_{TR} tricuspid valve resistance, C_{RA} right atrium compliance, R_{PU} pulmonary valve resistance

3D finite-element (FE) electromechanical model of the failing heart

The electromechanical model has two dynamic components, electrical and mechanical, as described previously [15]. Physiologically, as an electrical wave propagates through the heart, depolarization of each myocyte initiates release of calcium (Ca) from intracellular stores. This is followed by binding of the Ca to troponin C and cross-bridge cycling. The cross-bridge cycling forms the basis for contractile protein movement and the development of active tension in the cell, resulting in deformation of the ventricles.

The electrical component of the model simulates the propagation of a wave of transmembrane potential by solving the monodomain equations on the electrical mesh. This equation describes the current flow through cardiac cells that are connected electrically, enabling representation of a continuum. The current flow in the tissue is driven by active ion exchange across myocyte membranes. These processes are represented by the canine ionic model of Fox et al. [17]. Simultaneous solution of the partial differential equation (PDE) for the electrical conduction model and the set of ordinary differential equations (ODEs) for the ionic model represents simulation of electrical wave propagation in the heart.

A Ca transient serves as an input to the cell myofilament model representing the generation of active tension within each myocyte, in which a set of ODEs and algebraic equations describe Ca binding to troponin C, cooperativity between regulatory proteins, and cross-bridge cycling. Contraction of the ventricles results from the active tension generation represented by the model of myofilament dynamics of Rice et al. [18]. Deformation is described by the equations of passive cardiac mechanics, with the myocardium being an orthotropic, hyperelastic, and nearly incompressible material with passive properties defined by an exponential strain–energy function. Simultaneous solution of the myofilament model equations with those representing passive cardiac mechanics on the mechanical mesh constitutes simulation of cardiac contraction.

To take into account remodeling of the passive electromechanical properties associated with HF, changes were made to the electromechanical model. First, electrical conductivities were reduced by 30%, allowing for a total electrical activation time of 150 ms, according to the experimental results of Helm et al. [19]. To account for the increased stiffness of the failing myocardium, the passive scaling constant in the strain–energy function was increased fivefold [20]. Finally, to introduce systolic dysfunction, the peak of the calcium transient function ([Ca](t) of Eq. 55 in the myofilament model of Rice et al. [18]) which served as an input, was reduced to 70% of the normal value (Fig. 2a), and the time constant τ_2 was

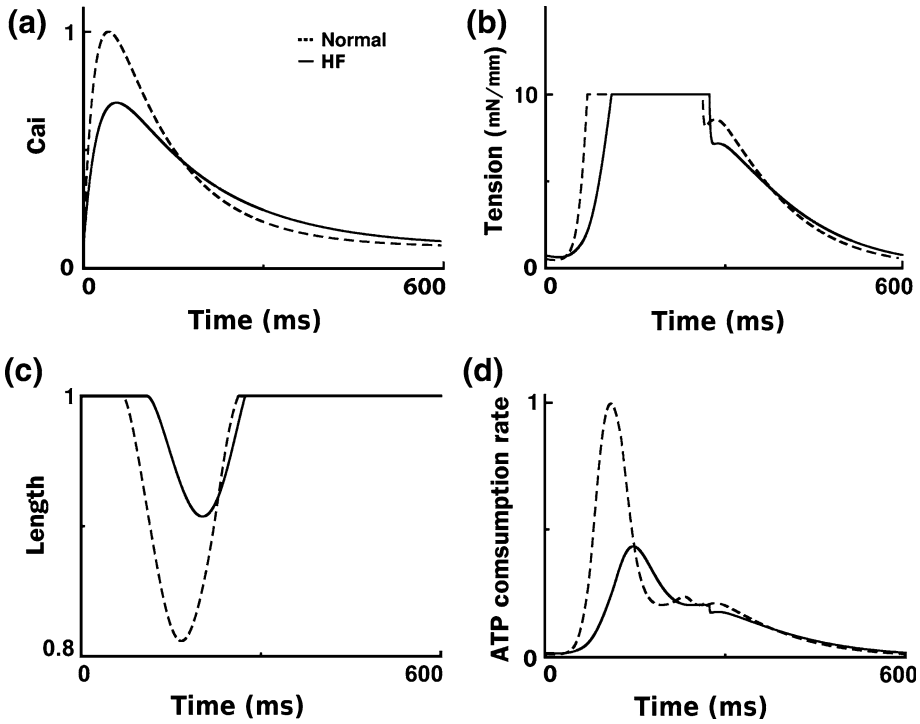

Fig. 2 Intracellular calcium transient Ca_i (**a**), myocardial tension (**b**), sarcomere shortening (**c**), and ATP consumption rate (**d**) as obtained from simulations with normal and HF models. The calcium transient is normalized by the peak calcium concentration under normal conditions. Sarcomere length is normalized by its value in the isometric contraction phase. The ATP consumption rate is normalized by the peak ATP consumption rate under normal conditions. *HF* denotes a heart failure patient

reduced by 30% of the normal value. This resulted in a calcium transient with a reduced peak and prolonged relaxation rate, which are the key features of the remodeled Ca transient in HF (Fig. 1D and 2C in O'Rourke et al. [21]). Figure 2b–d shows the simulated cellular tension, shortening, and contractile ATP consumption rate in normal and failing cardiomyocytes under isotonic contraction (10 kPa). The failing cardiomyocyte had a 42-ms delay in reaching the maximum tension, contracted 50% less, and consumed 55% less ATP than the normal cell under isotonic contraction. Here, the ejection fraction of the failed canine ventricle was approximately 14%.

The geometry of the failing canine ventricles was obtained from ex-vivo high-resolution magnetic resonance (MR) images. The unloaded volumes of the LV and right ventricle (RV) were calculated as functions of the degrees of freedom of the endocardial surface nodes using the divergence theorem. The unstressed volumes of the LV and RV were 69 and 46 ml, respectively. Fibers and laminar sheet structures were reconstructed from diffusion tensor (DT) MR cardiac images of the failing ventricles [15, 22]. The numerical methods for solving the equations of the electromechanical model have been described elsewhere [15, 23].

Combining the FE electromechanical model with the circulatory and LVAD models

Previously, we combined the FE electromechanical model of the failing ventricles with the lumped model of the circulatory system [15]. We also combined the full cardiovascular system model with the LVAD pump model [11]. The LVAD component was connected to the electromechanical and circulatory models through the inlet in the LV, and the outlet was attached to the aorta in the circulatory model. Briefly, the LVAD component was modeled as a flow generator with a specific mean flow rate of 40 ml/s for both continuous and pulsatile LVADs. Constant-flow conditions were used to simulate the continuous LVAD. In a previous study [11], the flow waveform of the pulsatile LVAD was taken from data measured for a specific pulsatile pneumatic LVAD to simulate the pulsatile LVAD. In contrast, in this study we used a harmonic function for the temporal waveform of the pulsatile LVAD in order to use a more general waveform for the various pulsatile LVADs. The flow waveform of the pulsatile LVAD using the harmonic function was calculated as follows:

$$LVAD\ inflow = \begin{cases} A\sin(\omega t), \ if (n\pi \le t < m\pi, \\ n : even\ number,\ m : odd\ number) \\ 0, \ else \end{cases} \quad (1)$$

$$LVAD\ outflow = \begin{cases} A\sin(\omega t + \pi), \ if\ (n\pi \le t < m\pi, \\ n : even\ number,\ m : odd \\ number) \\ 0, \ else \end{cases} . \quad (2)$$

The maximum flow rate, A, is 125 ml/s, which was calculated for the mean flow rate of 40 ml/s. The corresponding flow waveforms are shown in Fig. 3.

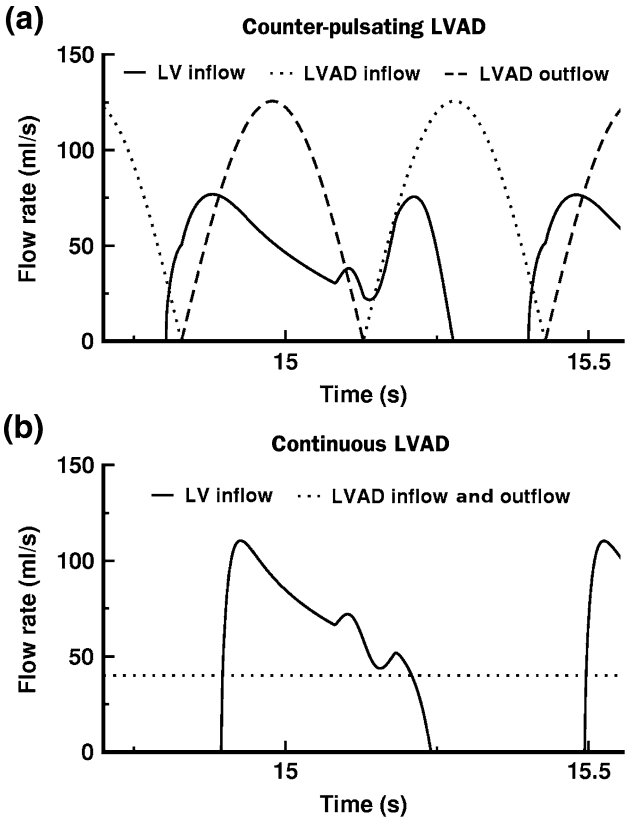

Fig. 3 Waveforms of the LV inflow and LVAD inflow and outflow under conditions of counter-pulsating LVAD support (**a**) and continuous LVAD support (**b**). The duration of the LVAD inflow and outflow is 300 ms. The duration of the LV inflow is 485 ms under counter-pulsating LVAD support and 365 ms under continuous LVAD support

Contractile ATP consumption of the myocardium

The contractile energy consumption of the myocardium was quantified by calculating the contractile ATP consumption in the myofilament model of Rice et al. [18]. The contractile ATP consumption rate, E, per unit volume was calculated as a function of the ATP-consuming cross-bridge detachment rate (g_{xbT}) and the single overlap fraction of thick filaments ($\mathrm{SOVF}_{\mathrm{Thick}}$),

$$E = g_{xbT} \times SOVF_{Thick}, \tag{3}$$

where g_{xbT}, which indicates the ATP-consuming detachment transition rate, and $\mathrm{SOVF}_{\mathrm{Thick}}$, which indicates the single-overlap fraction of the thick filament, were functions taken from the original myofilament model of Rice et al. [18].

Then, g_{xbT} can be derived as:

$$g_{xbT} = g_{xb} \times gxbmd \times xbmod_{species} \times Qg_{xb}^{\left(\frac{TmpC-37}{10}\right)}. \tag{4}$$

The term $xbmod_{\mathrm{species}}$ scales all cross-bridge cycling rates to account for species-based differences (0.2 for canines). The temperature dependence of g_{xbT} (Qg_{xb}) is set to a default Q_{10} value of 6.25. The term g_{xbT} had strain dependence in the rate modifier *gxbmd*, defined as:

$$gxbmd = \begin{cases} \exp\left(\sigma_p\left(\dfrac{x_0 - xXB_{PostR}}{x_0}\right)^2\right) & if\ xXB_{PostR} < x_0 \\ \exp\left(\sigma_n\left(\dfrac{x_0 - xXB_{PostR}}{x_0}\right)^2\right) & if\ xXB_{PostR} \geq x_0 \end{cases}, \tag{5}$$

where σ_{p} and σ_{n} set the effects of strain for positive and negative shortening velocities, respectively; x_0 is the distortion of the cross-bridge head; xXB_{PostR} is the mean distortion of states XB_{PostR}, which is the probability of transition to post-rotated force-generating status. The ATP-consuming detachment transition rate g_{xbT} is proportional to *gxbmd*, which depends on the strain of the cross bridges, and in turn, this strain depends on the velocity of contraction (for details see Rice et al. [18]). Finally, we calculated the ATP consumption distribution by integrating the ATP consumption rate with time for 600 ms and the ATP consumption of the entire ventricle by spatially integrating the local ATP consumption through the entire ventricular volume.

Simulation procedure

Ventricular contraction of the failing heart was simulated without an LVAD and with continuous and pulsatile LVAD support. For all simulations, the duration of the entire cardiac cycle was 600 ms. For the pulsatile LVAD, the pumping timing relative to activation of the ventricles was varied from 0 to 600 ms in 30-ms steps to find the optimum counter-pulsation condition. The contractile ATP consumption of the ventricle and pressure and volume unloading were calculated in each case and compared between continuous and pulsatile LVADs.

Results

Ventricular unloading in pressure and volume during LVAD support

Flow waveforms of the pulsatile and continuous LVADs and the LV inflow are shown in Fig. 3. All blood entered the LV through the mitral valve and exited via the LVAD, not through the aortic valve, because the LVAD provided full support. The period between mitral valve opening and closing was longer with counter-pulsating LVAD support (Fig. 3a) than with continuous LVAD support (Fig. 3b). The areas under the LV inflow curves under the continuous

and counter-pulsating LVAD conditions were the same (24 ml); this was used as the LV stroke volume.

Figure 4a–c illustrates the temporal pressure variation in the LV and systemic arteries for the three cases studied. In the model of HF without an LVAD (Fig. 4a), the mean arterial pressure was approximately 55 mmHg with 4-mmHg pulse pressure, which is inadequate for providing sufficient blood to the peripheral organs. The LV peak pressure (LVPP) was similar to the systolic arterial pressure. When the continuous LVAD was applied, the LVPP decreased to 32 mmHg (46% of the value for HF without an LVAD), whereas the arterial pressure greatly exceeded the LVPP, reaching 95 mmHg, which is in the normal range for canine blood pressure (Fig. 4b). The counter-pulsating LVAD generated a much lower LVPP (5.7 mmHg, 10% of the value for HF without an LVAD) and almost the same mean arterial pressure as the continuous-mode LVAD (Fig. 4c). For both types of LVAD, the ventricular pressure was always lower than the arterial pressure; therefore, the aortic valve was closed during the entire cardiac cycle, and all the blood left the ventricles through the LVAD.

Figure 4d shows the relative values of the LVPP, normalized by the value derived for HF without LVAD support, as a function of the delayed pumping time. The delayed pumping time on the *x*-axis is defined by the moment when the LVAD starts pumping blood out of the ventricle at the beginning of LV contraction. In the case of continuous LVAD pumping, the LVPP (normalized for the value for HF without an LVAD) was maintained at 0.46. From 180 to 420 ms, the LVPP for the case with a pulsatile LVAD was less than that for the continuous LVAD. Specifically, the pressure unloading effect ofthe pulsatile LVAD was maximum near 300 ms, which is part of diastole. The ventricular pressure waveform at 300 ms is depicted in Fig. 4c. These results are consistent with experimental results and simulations using the lumped model [11, 12], which found that the LV pressure decreased dramatically with LVAD support and that this reduction was more significant with the counter-pulsation LVAD.

Figure 5a–f shows active tension and the corresponding fiber strain at different wall depths of the LV free wall for the three cases studied: without LVAD support (Fig. 5a, b), with continuous LVAD support (Fig. 5c, d), and with counter-pulsating LVAD support (Fig. 5e, f). The active tension and end-diastolic strain decreased with LVAD support, especially with counter-pulsating LVAD support. Additionally, the active tension and fiber end-diastolic strain were highest at the endocardium and lowest at the epicardium; this trend was reported in a previous paper [15]. Figure 5g shows the pressure–volume curves for the three cases studied. No isovolumic contraction period was observed for both cases with LVAD support (dotted and dashed lines in Fig. 5g); this is because the LVAD ejected blood from the LV even during the period when both the mitral and aortic valves were closed. The pressure–volume curves shifted to the left and downward, and the end-diastolic volume decreased by 8 ml, indicating that the LVAD results in ventricular volume unloading by reducing the end-diastolic volume. The difference between the end-diastolic and end-systolic LV volumes was 16 ml for the counter-pulsating LVAD and 9 ml for the continuous LVAD. In general, with no LVAD support, the LV stroke volume can be calculated by subtracting the end-systolic LV volume from the end-diastolic LV volume. However, with LVAD support, the LV stroke volumes cannot be calculated in the same way—the real stroke volume of the LV

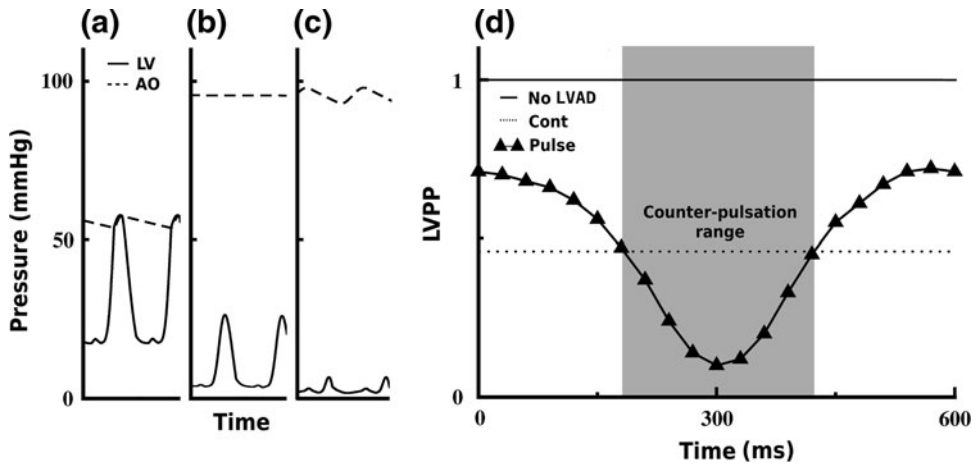

Fig. 4 Simulated pressure waveform in the LV and the systemic artery under HF conditions (**a**), and with the LVAD operating in continuous flow mode (**b**) or counter-pulsating mode (**c**). **d** The LVPP in the ventricles without an LVAD, and with continuous and pulsatile LVADs. LVPP is normalized by LVPP in the ventricles without LVAD support. The time axis indicates the delayed pumping time of the pulsatile LVAD from the beginning of ventricular contraction. *AO* aorta, *Cont* continuous LVAD, *Pulse* pulsatile LVAD

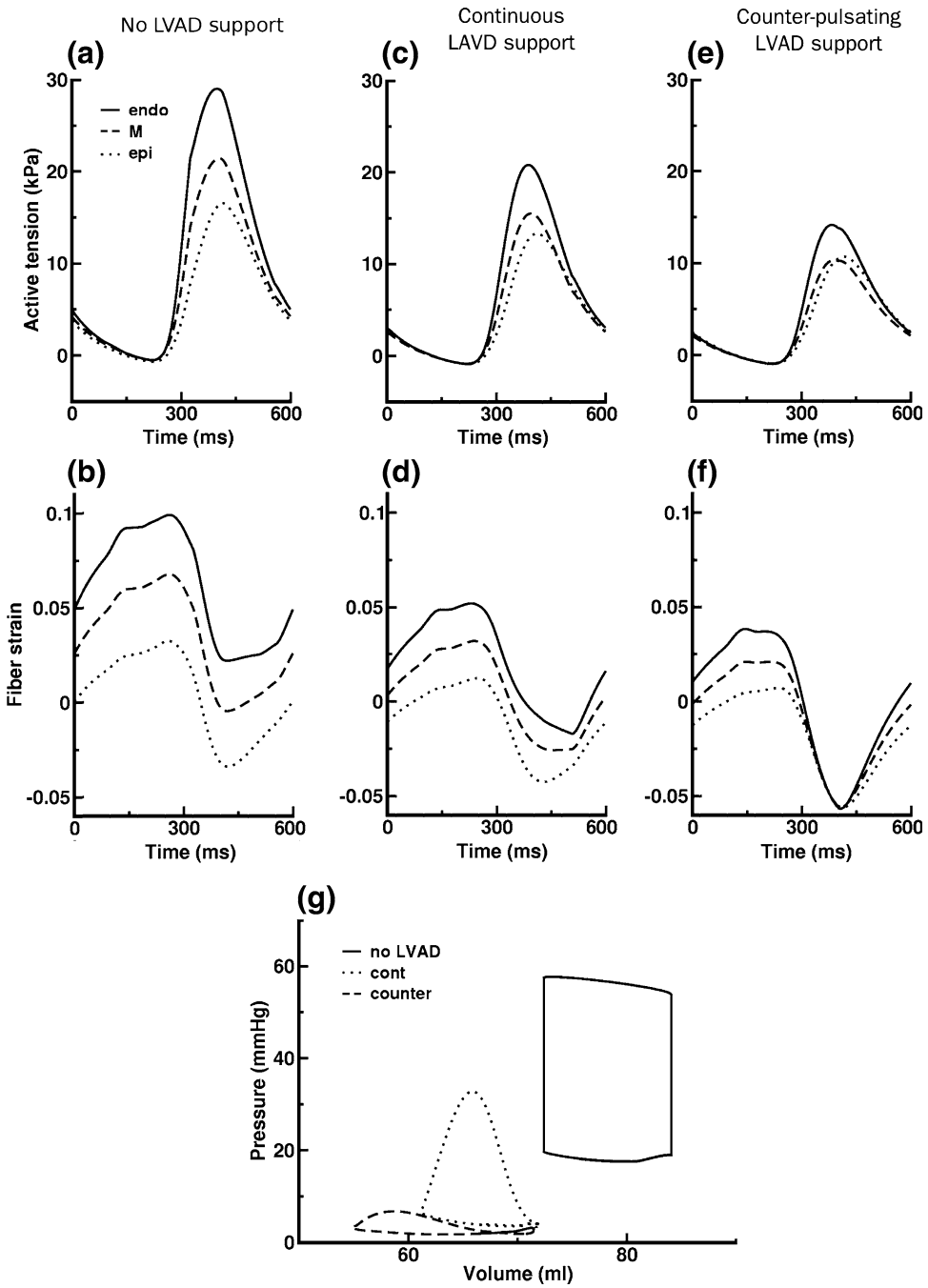

Fig. 5 Active tension and the corresponding fiber strain for different wall depths at mid-base of the posterior LV free wall: **a**, **b** without LVAD support; **c**, **d** with continuous LVAD support; and **e**, **f** with counter-pulsating LVAD support. The unstressed state is the reference state for the strain calculations. **g** The LV pressure–volume curves for HF without LVAD support, with continuous LVAD support, and with counter-pulsating LVAD support. *endo*, endocardium; *M* mid-myocardium, *epi* epicardium, *cont* continuous LVAD support, *counter* counter-pulsating LVAD support

supported by an LVAD is 24 ml, which was calculated by integrating the flow waveform through the mitral valve (Fig. 3). The LVAD pumps blood from the LV without considering the ventricular pumping status. The LVAD even pumps blood from the LV during the ventricular filling period; specifically, the continuous LVAD pumps blood all the time at a constant rate of 40 ml/s (Fig. 3). This is why the stroke volume of the LV supported by an LVAD is not as same as the difference between the end-diastolic and end-systolic volumes of the LV.

Ventricular unloading assessed by myocardial energy consumption

Figure 6a–c shows the calculated transmural distribution of the contractile ATP consumption rate at end systole for HF without an LVAD (Fig. 6a), the model with the LVAD operating in continuous pumping mode (Fig. 6b), and that operating in counter-pulsating mode (Fig. 6c). The contractile ATP consumption decreased significantly in the presence of either LVAD, especially with the counter-

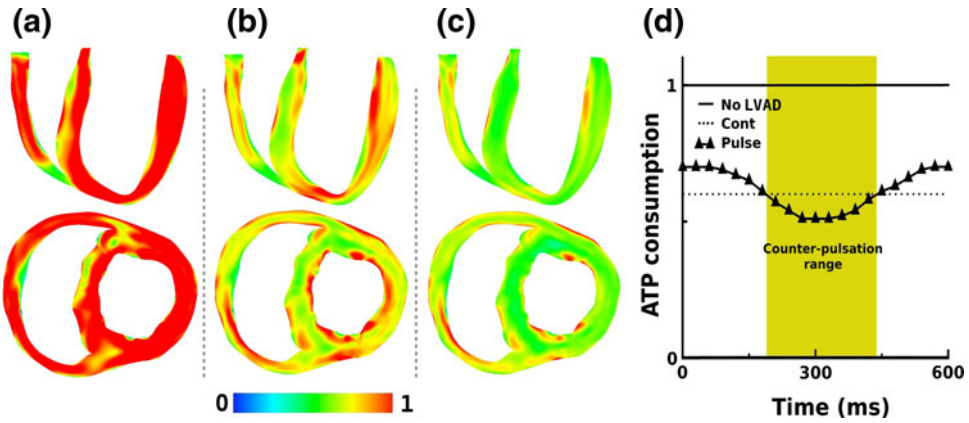

Fig. 6 Transmural distribution of ATP consumption rate in HF ventricles with no support (**a**), with continuous LVAD (**b**), and with counter-pulsating LVAD (**c**). **d** Total ATP consumption in the ventricles without LVAD, and with continuous and pulsatile LVADs. ATP consumption is normalized by the ATP consumption of the ventricles without LVAD support. The time axis indicates the pumping phase for the pulsatile LVAD. *Cont* Continuous LVAD, *Pulse* pulsatile LVAD

pulsating LVAD support. The contractile ATP consumption of both ventricles as a function of the pulsatile LVAD pumping timing is shown in Fig. 6d. The values for contractile ATP consumption were normalized using those from the case with no LVAD support. Compared with the case of HF without an LVAD, contractile ATP consumption decreased by 40% with continuous LVAD support and by as much as 50% with counter-pulsating LVAD support. Although the ATP consumption curves for the three cases were similar (in overall trend) to the LVPP curves (Fig. 4d), the effect of the counter-pulsatile LVAD on the LVPP was much more pronounced than the effect of the counter-pulsatile LVAD on contractile ATP consumption. Specifically, the counter-pulsating LVAD was 36% more effective in reducing the LVPP than was the continuous LVAD, but only 10% more effective in reducing contractile ATP consumption by the myocardium.

Discussion

This study used a sophisticated computational approach to compare the effect of continuous and pulsatile LVADs on ventricular unloading. The main findings were that:

1. pressure unloading is greater with a pulsatile LVAD than with a continuous LVAD;
2. reductions in end-diastolic volume were the same for both LVADs;
3. both LVADs resulted in significant decreases in contractile ATP consumption; and
4. the difference between reduction of contractile ATP consumption in the two LVAD modes was much smaller than the difference between the reduction in LVPP in the two modes.

The electromechanical model presented here is a new approach for understanding the benefits of LVADs, particularly in regard to hemodynamics and the contractile energy consumption of the myocardium. To our knowledge, this is the first image-based electromechanical model coupled to a detailed representation of an LVAD system. The model also features a new formulation of contractile ATP consumption by the local myocardium that is based on myofilament dynamics. Moreover, we incorporate an anatomically accurate geometry of the failing canine heart and physiologically accurate modifications to both the electrical and mechanical properties of the ventricles to reflect the electromechanical remodeling associated with HF.

Both LVAD types reduced LVPP, end-diastolic LV volume, and contractile ATP consumption significantly. However, under optimum counter-pulsating conditions (300-ms pumping time in Figs. 4d, 6d), the reduction in the LVPP with the continuous LVAD was 36% less than that with the pulsatile LVAD, whereas the reduction in contractile ATP consumption with the continuous LVAD was only 10% less than that with the pulsatile LVAD. This stems from the fact that the working myocardium consumes energy when the ventricles contract and that a fraction of this energy is not affected by pressure unloading irrespective of the type of LVAD. Our simulation results demonstrate that approximately 50% of the total energy consumed in each cycle by the failing heart is transformed into end-systolic potential energy stored in mechanical deformations of the ventricular walls. Suga et al. [24] showed experimentally for the normal canine heart that this fraction can be estimated as approximately 20% of the total energy consumed. The fraction is greater for the failing heart because of the reduced active tension. The end-

systolic potential energy is calculated by subtracting the external mechanical work, the quasi-rectangular area within the pressure–volume loop trajectory, from the ventricular systolic pressure–volume area [24].

This study found that the contractile ATP consumption varied transmurally. In general, the sarcomere length affects the density of effective cross-bridges and therefore the contractile force; this is known as the Frank–Starling law of the heart. Therefore, a longer sarcomere length results in greater contractile ATP consumption because of the greater density of the attached cross bridges in myocytes, as expressed in Eq. 3. Previously, we demonstrated that myofibers in the endocardium have greater end-diastolic lengths than myofibers in the mid-myocardium and epicardium [15]. Figure 5 also shows that the end-diastolic strain and active tension of the endocardial sarcomere is greatest, irrespective of the type of LVAD support. This explains why contractile ATP consumption by the endocardium was greater than that at the mid-wall or epicardium (Fig. 6a–c). In the absence of LVAD support, greater dependence of fiber strain on depth in the wall (Fig. 5) was observed in this study than in the previous reports by Ashikaga et al. [25] and Rodriguez et al. [26]. However, several conditions in our model were different from those in their experiments. First, our model was based on a failed heart whereas they used an intact canine heart. Second, we used the unloaded state of LV as the reference condition for strain calculation in this study, but end-diastolic volume was regarded as the reference in the previous experiments.

The pumping timing of the pulsatile LVAD affected the LVPP and contractile ATP consumption. The pulsatile LVAD performed better than the continuous LVAD in reducing the LVPP and contractile ATP consumption during the effective counter-pulsation period, as shown in Figs. 4d, 6d, whereas it performed worse outside of this range, i.e., with co-pulsation. Therefore, it is important to synchronize the pumping phase of a pulsatile LVAD with the LV as counter-pulsation.

Clinical implications

The reduction in the LVPP, i.e., the pressure unloading, has been used clinically for estimation of myocardial recovery during LVAD support [27]. The reduction in contractile ATP consumption, i.e., the energy unloading effect, is more directly related to cardiac recovery than are the ventricular pressure and volume unloading. It is well known that the intracellular ATP concentration in the failing heart decreases because of reduced capability of ATP production by mitochondria [28]. This can induce plasma membrane permeabilization and cell rupture, easily causing necrosis. Therefore, the decrease in ATP consumption as a result of LVAD support helps the failing myocardium to recover by suppressing the decrease of intracellular ATP concentration. Besides, according to the experiment of Lee et al. [29], the decrease in ATP consumption as a result of LVAD support results in reduced oxygen consumption by mitochondria and helps myocardium recovery by suppressing further ischemic damage. Our study found that the counter-pulsating LVAD resulted in less energy unloading than pressure unloading. Unlike the contractile ATP consumption, the reduction in the LVPP may not predict myocardial recovery accurately. Moreover, the finding that contractile ATP consumption differed by less than 10% for the two LVAD types might explain the comparable myocardial recovery for patients with continuous and counter-pulsating LVADs in clinical trials [13]. However, there is another possibility that the change of mechanical stress induces long-term cellular remodeling which could affect myocardial function and, eventually, clinical outcome [13].

Limitations

We used an image-based electromechanical model of failing canine ventricles. Previous studies of myocardial recovery resulting from LVAD use were performed for patients whose ventricular geometry, fiber architecture, and hemodynamics differ from those of canine ventricles [4–6]. Also, we considered only the contractile ATP consumption of the myocardium, although ATP is used in other ways, for example by sarcoplasmic/endoplasmic reticulum calcium ATPase (SERCA), plasma membrane Ca^{2+}-ATPase (PMCA), and Na pumps. Last, to reduce modeling complexity we did not implement the coronary circulation. However, these limitations are not expected to greatly alter the main findings of this study.

Acknowledgments This work was supported by the NRL (National Research Laboratory) program of the National Research Foundation of Korea (No. ROA-2008-000-20127-0), and grant from NIH (R01 HL0882729 to NAT and F31 HL103090 to JLC) and NSF (CBET-0933029 to NAT).

References

1. Casarotto D, Bottio T, Gambino A, Testolin L, Gerosa G (2003) The last to die is hope: prolonged mechanical circulatory support with a Novacor left ventricular-assist device as a bridge to transplantation. J Thorac Cardiovasc Surg 125:417–418
2. John R, Kamdar F, Liao K, Colvin-Adams M, Boyle A, Joyce L (2008) Improved survival and decreasing incidence of adverse events with the HeartMate II left ventricular-assist device as bridge-to-transplant therapy. Ann Thorac Surg 86:1227–1234 (discussion 1234–5)
3. Daneshmand MA, Rajagopal K, Lima B, Khorram N, Blue LJ, Lodge AJ, Hernandez AF, Rogers JG, Milano CA (2010) Left ventricular-assist device destination therapy versus extended

criteria cardiac transplant. Ann Thorac Surg 89:1205–1209 (discussion 1210)
4. Altemose GT, Gritsus V, Jeevanandam V, Goldman B, Margulies KB (1997) Altered myocardial phenotype after mechanical support in human beings with advanced cardiomyopathy. J Heart Lung Transpl 16:765–773
5. Levin HR, Oz MC, Chen JM, Packer M, Rose EA, Burkhoff D (1995) Reversal of chronic ventricular dilation in patients with end-stage cardiomyopathy by prolonged mechanical unloading. Circulation 91:2717–2720
6. Barbone A, Oz MC, Burkhoff D, Holmes JW (2001) Normalized diastolic properties after left ventricular assist result from reverse remodeling of chamber geometry. Circulation 104:I229–I232
7. Nakatani S, McCarthy PM, Kottke-Marchant K, Harasaki H, James KB, Savage RM, Thomas JD (1996) Left ventricular echocardiographic and histologic changes: impact of chronic unloading by an implantable ventricular-assist device. J Am Coll Cardiol 27:894–901
8. Sezai A, Shiono M, Orime Y, Nakata K, Hata M, Nemoto M, Saitoh T, Sezai Y (1996) Comparison studies of major organ microcirculations under pulsatile- and nonpulsatile-assisted circulations. Artif Organs 20:139–142
9. Klotz S, Deng MC, Stypmann J, Roetker J, Wilhelm MJ, Hammel D, Scheld HH, Schmid C (2004) Left ventricular pressure and volume unloading during pulsatile versus nonpulsatile left ventricular-assist device support. Ann Thorac Surg 77:143–149 (discussion 149–50)
10. Drews T, Jurmann M, Michael D, Miralem P, Weng Y, Hetzer R (2008) Differences in pulsatile and non-pulsatile mechanical circulatory support in long-term use. J Heart Lung Transpl 27:1096–1101
11. Lim KM, Kim IS, Choi SW, Min BG, Won YS, Kim HY, Shim EB (2009) Computational analysis of the effect of the type of LVAD flow on coronary perfusion and ventricular afterload. J Physiol Sci 59:307–316
12. Shi Y, Korakianitis T, Bowles C (2007) Numerical simulation of cardiovascular dynamics with different types of VAD assistance. J Biomech 40:2919–2933
13. Garcia S, Kandar F, Boyle A, Colvin-Adams M, Lliao K, Joyce L, John R (2008) Effects of pulsatile- and continuous-flow left ventricular-assist devices on left ventricular unloading. J Heart Lung Transpl 27:261–267
14. Sarnoff SJ, Braunwald E, Welch GH Jr, Case RB, Stainsby WN, Macruz R (1958) Hemodynamic determinants of oxygen consumption of the heart with special reference to the tension-time index. Am J Physiol 192:148–156
15. Gurev V, Lee T, Constantino J, Arevalo H, Trayanova NA (2011) Models of cardiac electromechanics based on individual hearts imaging data: image-based electromechanical models of the heart. Biomech Model Mechanobiol 10:295–306
16. Jie X, Gurev V, Trayanova N (2010) Mechanisms of mechanically induced spontaneous arrhythmias in acute regional ischemia. Circ Res 106:185–192
17. Fox JJ, McHarg JL, Gilmour RF Jr (2002) Ionic mechanism of electrical alternans. Am J Physiol Heart Circ Physiol 282:H516–H530
18. Rice JJ, Wang F, Bers DM, de Tombe PP (2008) Approximate model of cooperative activation and crossbridge cycling in cardiac muscle using ordinary differential equations. Biophys J 95:2368–2390
19. Helm RH, Byrne M, Helm PA, Daya SK, Osman NF, Tunin R, Halperin HR, Berger RD, Kass DA, Lardo AC (2007) Three-dimensional mapping of optimal left ventricular pacing site for cardiac resynchronization. Circulation 115:953–961
20. Wu Y, Bell SP, Trombitas K, Witt CC, Labeit S, LeWinter MM, Granzier H (2002) Changes in titin isoform expression in pacing-induced cardiac failure give rise to increased passive muscle stiffness. Circulation 106:1384–1389
21. O'Rourke B, Kass DA, Tomaselli GF, Kaab S, Tunin R, Marban E (1999) Mechanisms of altered excitation-contraction coupling in canine tachycardia-induced heart failure, I: experimental studies. Circ Res 84:562–570
22. Vadakkumpadan F, Arevalo H, Prassl AJ, Chen J, Kickinger F, Kohl P, Plank G, Trayanova N (2010) Image-based models of cardiac structure in health and disease. Wiley Interdiscip Rev Syst Biol Med 2:489–506
23. Provost J, Gurev V, Trayanova N, Konofagou EE (2011) Mapping of cardiac electrical activation with electromechanical wave imaging: an in silico-in vivo reciprocity study. Heart Rhythm 8:752–759
24. Suga H, Hisano R, Goto Y, Yamada O, Igarashi Y (1983) Effect of positive inotropic agents on the relation between oxygen consumption and systolic pressure volume area in canine left ventricle. Circ Res 53:306–318
25. Ashikaga H, Omens JH, Ingels NB Jr, Covell JW (2004) Transmural mechanics at left ventricular epicardial pacing site. Am J Physiol Heart Circ Physiol 286:H2401–H2407
26. Rodriguez EK, Hunter WC, Royce MJ, Leppo MK, Douglas AS, Weisman HF (1992) A method to reconstruct myocardial sarcomere lengths and orientations at transmural sites in beating canine hearts. Am J Physiol 263:H293–H306
27. Burkhoff D, Klotz S, Mancini DM (2006) LVAD-induced reverse remodeling: basic and clinical implications for myocardial recovery. J Card Fail 12:227–239
28. Marin-Garcia J, Goldenthal MJ (2008) Mitochondrial centrality in heart failure. Heart Fail Rev 13(2):137–150
29. Lee SH, Doliba N, Osbakken M, Oz M, Mancini D (1998) Improvement of myocardial mitochondrial function after hemodynamic support with left ventricular-assist devices in patients with heart failure. J Thorac Cardiovasc Surg 116(2):344–349